Int J Adv Manuf Technol (2018) 94:2199–2207
DOI 10.1007/s00170-017-1019-1

ORIGINAL ARTICLE

Influence of laser exposure time and point distance on 75-μm-thick layer of selective laser melted Alloy 718

P. Karimi[1] · T. Raza[1] · J. Andersson[1] · L.-E. Svensson[1]

Received: 13 May 2017 / Accepted: 22 August 2017 / Published online: 6 September 2017

Abstract A systematic matrix with 25 samples, using five different point distances and five laser exposure times, depositing 75-μm-thick layers of Alloy 718 has been studied. The work has concentrated on defects formed, hardness of the deposits, and the microstructure. Relatively large amount of defects, both lack of fusion and porosity, was found in several of the specimens in the deposits. The defects were never possible to fully eliminate, but a significant decrease, mainly in the lack of fusion, was seen with increasing laser exposure time. The gas porosity on the other hand was not affected to any larger degree, except for the lowest laser energy input, where a slight increase in porosity was seen. A small increase in hardness was noted with increasing laser energy input. The width of the deposited beads increased with increasing laser energy, while the depth of deposits was more or less constant. However, for the lowest combination of point distance and laser exposure time, quite deep and narrow beads were formed. A comparison was made with deposition of 50-μm-thick layers, with quite similar laser energy input, but with some variation in detailed deposition parameters. It was found that the 75-μm-thick layers contained less lack of fusion, particularly for small point distances. The amount of porosity was also less, but that did not vary with deposition parameters.

Keywords Additive manufacturing · Selective laser melting (SLM) · Alloy 718 · Microstructure · Hardness

✉ P. Karimi
paria.karimi-neghlani@hv.se

[1] Department of Engineering Science, University West, 461 53 Trollhättan, Sweden

1 Introduction

Several studies have been performed to evaluate the microstructures and mechanical properties of SLM processed Alloy 718 parts, for example [1–5]. Studies have reported the effects of laser power [5, 6], scanning speed [6], scanning strategy [7], and laser energy density [5, 6] on microstructure and mechanical characteristics of Alloy 718. In SLM-manufactured parts, the desired microstructure is necessarily influenced by complex chemical and physical behaviors through the melt pool as a result of non-equilibrium laser processing technique [8]. To fully understand these effects, significant investigations are still needed to focus on microstructures and properties of the as-manufactured parts under different processing conditions.

One of the main process parameter during SLM deposition is laser energy density which, for example, controls densification features of Alloy 718 parts. The densification level is reduced at relatively low laser energy density, due to the formation of open pores and balling effect [6, 9, 10].

In another paper, the effects of different laser scanning speeds on the densification and microstructure properties of Alloy 718 parts produced by SLM were described [11]. It was confirmed that the Alloy 718 parts were successfully fabricated with scanning speeds ranging from 100 to 1600 mm/s. However, the highest density of the parts (99.7%) was obtained with the laser scanning speed 800 mm/s, which produced good metallurgical bonding without critical defects. The optimally processed Alloy 718 parts revealed a uniform hardness distribution with an average value of 320 $HV_{0.5}$. In terms of microscopic properties, the microstructure of as-built Alloy 718 parts predominantly consisted of columnar grains across multiple layers, where they were oriented near-parallel to the building direction [11].

However, more investigations are needed to fully understand the relationship between the processing parameters,

microstructures, and properties of the as-fabricated parts. Furthermore, there is a lack of knowledge about the influences of laser exposure time and point distance on the microstructure and properties of SLM-deposited Alloy 718 which need to be investigated. Thus, the aim of the present work is to clarify this. A number of papers [12–14] present research into how layer thickness influences the microstructure and properties of parts obtained on the basis of the SLM technology. However, no research has been made into comparison of the characteristics of samples manufactured with the use of layer thickness equal to 50 and 75 μm for Alloy 718. A similar study was recently made for a 50-μm-thick layer [15]. In the present paper, a 75-μm-thick layer is investigated and comparison between the two layer thicknesses will be made.

2 Materials and experimental work

2.1 Powder feedstock

Gas-atomized Alloy 718 powder was used as feedstock. It was supplied by LPW Technology, having a spherical shape and particle size distribution in a range of 15–45 μm. The chemical composition of the Alloy 718 powder is given in Table 1.

2.2 Laser processing

SLM manufacturing of a 5 × 5 matrix of cubic samples with dimension of 10 × 10 × 10 mm^3 was performed using a Renishaw AM 250 system equipped with a 200-W SPI Ytterbium fiber laser. An overall picture of all 25 cubes in the test matrix is shown in Fig. 1 in chapter 3.1. All cube samples were produced with varying exposure time and point distance, keeping the other process parameters constant. The samples were investigated directly after SLM processing, without any subsequent heat treatments. The energy input normally given for this process is based on Eq. 1:

$$E = \frac{P}{\frac{Point\ distance}{Exposure\ time} \times Layer\ thickness \times Hatch\ distance} \quad (1)$$

where E is energy (J/mm^3), P is power (W), point distance is the distance between the deposited spots (mm), exposure time is the time the laser is heating on one spot (s), layer thickness is the original thickness of the deposited layer (mm), and hatch distance is the distance between two adjacent scaning rows (mm).

In the present case, P is 200 W, layer thickness is 0.075 mm, and hatch distance 0.1 mm. Point distance and exposure time will vary and consequently then also the supplied energy. The process parameters are given in Table 2 and the resulting energy input in Table 3.

2.3 Specimen preparation

As shown in Fig. 2, the cubic samples were cut from the normal reference plane (indicated by the dashed line) in parallel to the build direction and then polished down to a grit size of 1 μm. Finally, the polished samples were etched using Kalling's solution (40 ml of HCl + 2 g of $CuCl_2$ + 80 ml of methanol) at room temperature for 3 to 5 s.

2.4 Characterization of microstructure

The microstructure of all samples was investigated by optical microscopy (OM). For each sample, 16 images (100× magnification) were taken in the normal reference plane in order to examine defects such as porosity and lack of fusion. The defects were quantitatively determined by point counting [16].

A Hitachi scanning electron microscope (TM3000, Tokyo, Japan), equipped with an EDS system, was used to study the microstructure and its phase constituents such as Laves phase and metallic carbides.

Vickers micro hardness ($HV_{0.5}$) measurements were taken using a micro hardness tester (HMV-2, Shimadzu, Tokyo, Japan) with an applied load of 500 g and a dwell time of 15 s. In order to perform hardness analysis along with build direction, ten micro hardness tests were performed for the samples in both top and bottom layers.

3 Results

3.1 General outlook of the samples

The general outlook of the 25 samples is shown in Fig. 1. Although not very clearly seen, there is a tendency that the porosity level is much lower in specimens in the upper left corner, like specimen A1 (40 μm point distance, 180 μs exposure time), while considerably more porosity is seen in the lower left corner, like specimen A5 (65 μm point distance, 180 μs exposure time). Occasionally, large porosities are seen also for longer exposure times, but in general the porosity

Table 1 Chemical compositions of Alloy 718 powder (wt%)

Element	Ni	Co	Cr	Mo	Ti	Al	Fe	Si	Cu	C	Nb+Ta
Wt%	Bal.	0.08	18.92	3.03	0.90	0.48	18.18	0.04	0.02	0.05	5.11

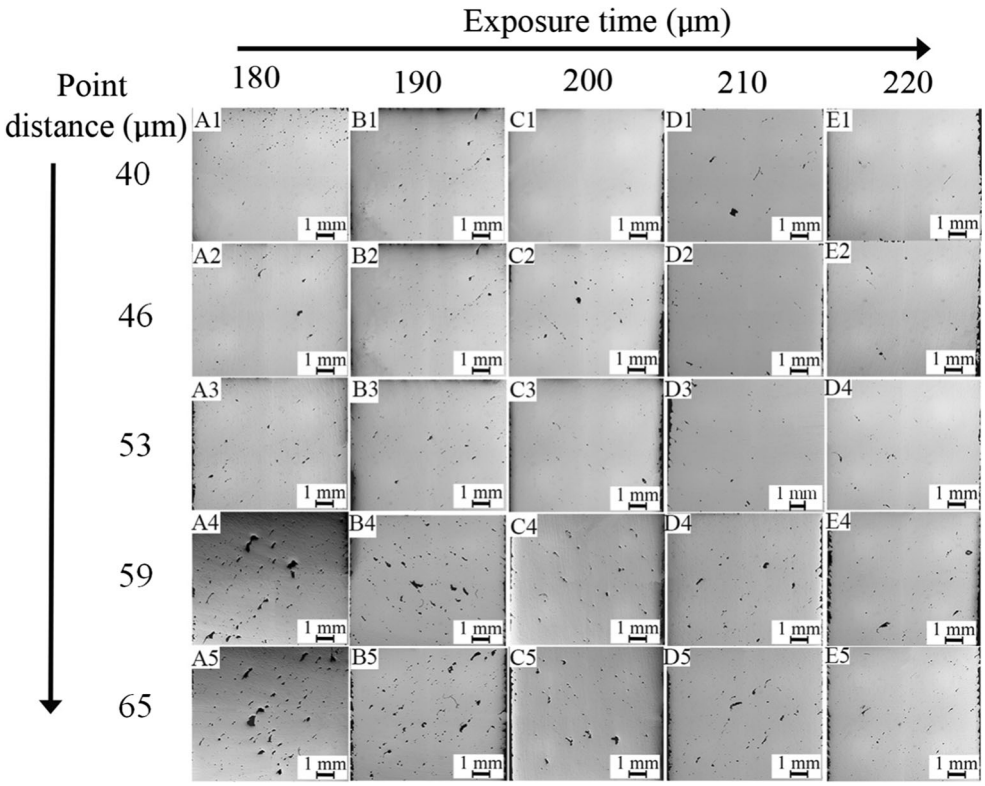

Fig. 1 Optical microscopy images of all 25 samples using different laser exposure time (μs) and point distance (μm)

content is decreasing with increased exposure time for all point distances. Consequently, it seems as the best choice is to have small point distance and long exposure time.

Figure 3a shows a relatively large gas porosity, found in the specimen deposited with 53 μm point distance and 180 μs exposure time. In the same figure, a lot of smaller porosities are also seen, although hardly visible. These small pores are assumed to be porosities being present in the powder already, while the large one shown in Fig. 3a is assumed to be formed during the SLM process. Figure 3b shows a lack of fusion defect in the specimen deposited with 59 μm point distance and 180 μs exposure time. Some large loosely held un-melted powder particles partly filling the lack of fusion can also be seen.

Increasing laser exposure time and decreasing laser point distance were expected to both reduced the presence of gas porosity and lack of fusion. This was certainly seen for laser point distance. However, the benefits from increased laser exposure time were mainly seen for higher point distances, while for lower point distances, the defect level was on the whole low, but with some variations. Another possibility is to compare the defect amount for different energy inputs.

In Fig. 4, it is shown how increasing the laser energy input (taking both exposure time and point distance into account) decreased the porosity. However, it should be noted that the

Table 2 Process parameters used in manufacturing of Alloy 718 (a) constant parameters, (b) variable parameters

(a)	
Laser power (W)	200
Spot size (μm)	80
Layer thickness (mm)	0,075
Hatch distance (mm)	0.1
Pre-heating temperature (°C)	150
Scan strategy	Alternating with 90 degree
(b)	
Exposure time (μs)	Point distance (μm)
180	40
190	46
200	53
210	59
220	65

Table 3 Laser energy input (J/mm^3) for the different process parameters

Point distance [μm]	Exposure time [μs]				
	180	190	200	210	220
40	120	127	133	140	147
46	104	110	116	122	128
53	91	96	101	106	111
59	81	86	90	95	99
65	74	78	82	86	90

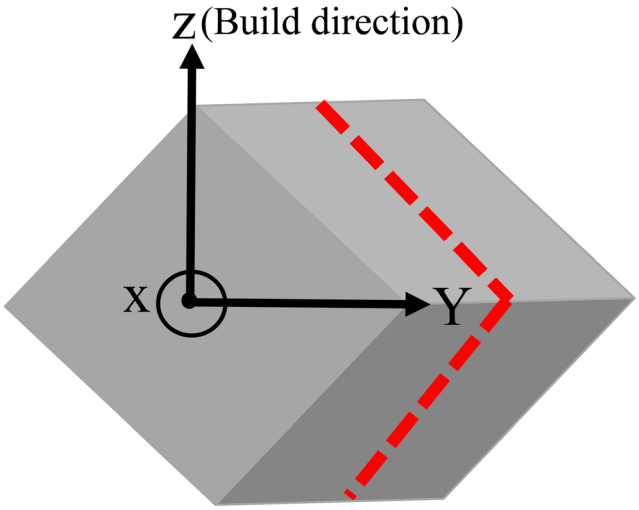

Fig. 2 Fabricating and sample cutting (red plane) orientation of the SLM as-manufactured samples

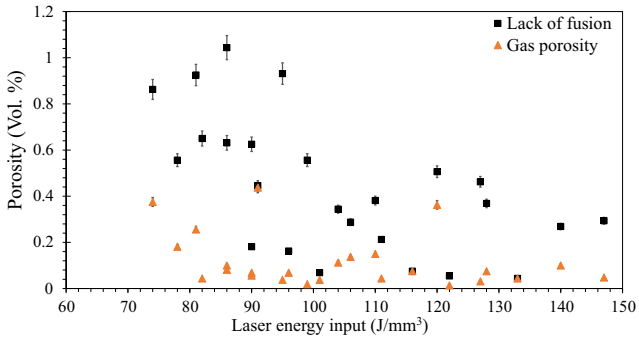

Fig. 4 Comparison between gas porosity and lack of fusion values at different laser energy input (J/mm^3)

gas porosity is affected to a very small degree, while lack of fusion is significantly affected. The large scatter in the lack of fusion defects can also be noted.

The gas porosity value for the lowest laser energy input (74 J/mm^3) was high (around 0.4%). However, in general, it was found that increasing laser energy decreased the amount of gas porosity. Overall, the gas porosity content was below 0.2%.

The main defect found was the lack of fusion. Some high values (0.8–1.2%) were found for lower energy inputs. It should though be noted that the really low values of lack of fusion are found, not for the highest laser energy, but for intermediate values. The positions B3, C1, C2, C3, D2, and E5 had the smallest amount of lack of fusion.

3.2 Effect of process parameters on hardness

The effect of point distance and exposure time on hardness was measured but it was difficult to find any clear relationships. A slightly increased hardness was found for the lower point distances using constant exposure times. However, the scatter in hardness was also quite large. If the hardness is plotted as function of laser energy input (Fig. 5), then a slight increase is seen with increased energy input. However, the increase is not very large, from around 290 to 320 $HV_{0.5}$.

3.3 Microstructure

The general microstructure for the four specimens at the corners of the experimental matrix (A1 = 40/180, 120 J/mm^3; A5 = 65/180, 74 J/mm^3; E1 = 40/220, 147 J/mm^3; E5 = 65/220, 90 J/mm^3) is shown in Fig. 6. The diameter of the deposited beads has been tried to be estimated, although it is fairly difficult and must be taken by caution. Examples of measured diameters are shown in Fig. 6. The correlation with the heat input is shown in Table 4 below. What is clearly seen here is that a longer exposure time gives wider beads and, in that case, there is very little sensitivity to point distance. However, for the shortest exposure time (180 μs), the point distance seemed to be very important. For some reason, which is still not understood, for a small point distance and a short

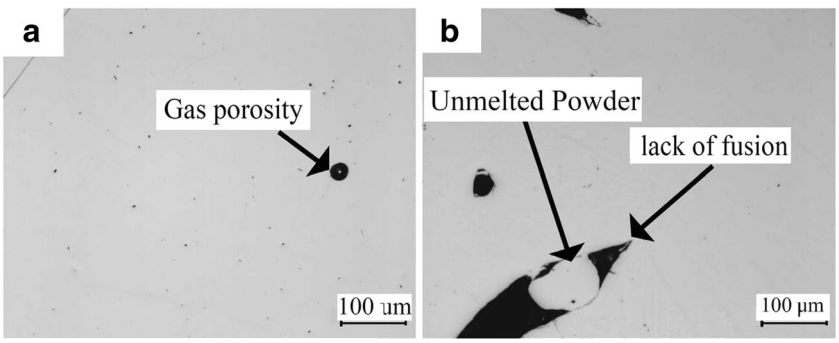

Fig. 3 Optical microscopy images of gas porosity and lack of fusion in different process condition. **a** 53 μm point distance and 180 μs exposure time (laser energy input 91 J/mm^3). **b** 59 μm point distance and 180 μs exposure time (laser energy input 81 J/mm^3)

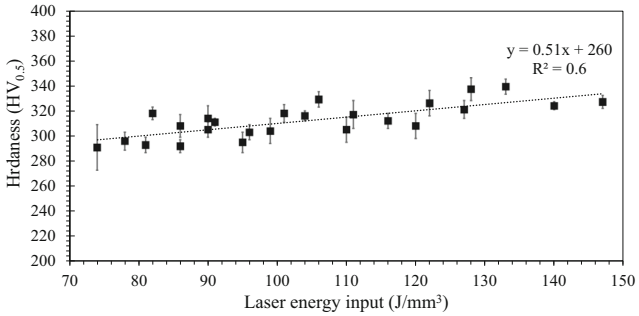

Fig. 5 Relationship between micro hardness and laser energy input of all different samples

exposure time, the beads became less wide but deeper. A larger point distance gave beads almost as wide as those deposited with a longer exposure time.

Micrographs of five samples with different laser exposure times (180, 190, 200, 210, and 220 μm) but with same point distance (40 μm) are presented in Fig. 7 (thus, A1 and E1 are the same as shown in Fig. 6). It illustrates that with larger laser exposure time, the laser energy input is increasing as well, making the width of melt pool wider. The mean value for width of melt pool showed an increasing trend from around 150 ± 16 to 290 ± 18 μm by increasing the laser exposure time.

Figure 8 shows the columnar grain structure along the building direction for the sample C1 (133 J/mm^3). As can be seen, there is mainly a columnar dendritic growth mode, but the secondary arms are seldom well developed.

The top layers disclosed relatively coarse columnar dendrites whereas the bottom layers showed narrow and uniformly distributed columnar dendrites along the build direction, as seen in Fig. 9a, b. The widths of columnar dendrite arm spacing in top and bottom layers were around 1.3 ± 0.4 and 0.8 ± 0.2 μm, respectively. The bottom layers had direct contacts with the substrate plate. The substrate plate had lower temperature and a significantly higher thermal conductivity in comparison to the melt pool; thus, bottom layers had higher cooling rate. Consequently, as expected, finer columnar grains were formed in the first layer of the deposit.

Nb micro-segregation occurred in the microstructure. The dendrite core areas were rich in Cr, Fe, and Ni and had lower values of Nb. Conversely, the interdendritic areas were rich in Nb. Nb micro-segregation was evident in all of the different samples in this study. No clear trend was found between scanning speed and degree of Nb segregation; however, there were slightly higher values of Nb segregation for higher laser scanning speed.

4 Discussion

In this discussion, the individual results of 75-μm bead thickness will be discussed and a comparison with 50 μm specimens, from another recent investigation (Raza et al. [15]), will be made. The points covered are the defects formed in the process, the hardness of the samples, and the microstructure of the deposited beads.

The defects found were lack of fusion and pores. Obviously, a longer laser exposure time gave less lack of fusion, however, with relatively large scatter. Moreover, the lack of fusion defects never completely disappeared. Since these defects were relatively large, it is questionable if they can be closed by further processing, like hot isostatic pressing (HIP) [17]. Thus, there must be a high focus of finding process parameters which can guarantee deposits free from the lack of fusion.

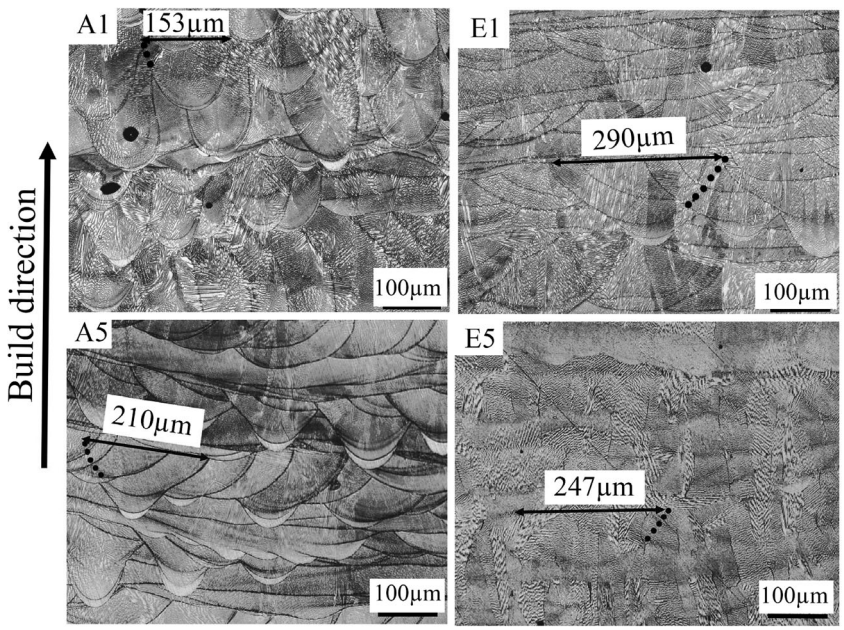

Fig. 6 Micrograph of the four samples A1, A5, E1, and E5, with the bead size indicated

Table 4 Bead size as a function of heat input for the four samples in Fig. 6

	A5 = 65/180	E5 = 65/220	A1 = 40/180	E1 = 40/220
Heat input (J/mm3)	74	90	120	147
Bead size (μm)	210	247	153	290

One possible mechanism, by which the lack of fusion defects can form, is from sintering of the powder particles during the deposition process, rather than melting together in result of low laser energy input. It is also possible that spattering may occur, for higher laser energies [6, 18, 19]. However, it is questionable whether that stage was reached in the present process. No report of this phenomenon was issued during manufacturing of the samples.

The gas porosity is assumed to be a smaller problem, partly since pores are more easily closed by HIP [17, 20], partly because pores seldom give rise to any significant problems during operations. However, it was noticed that some porosity obviously was forming during the SLM processing, in contrast to the majority of pores, which were inherited from porosity of the powder [21].

However, comparing the present results to the one of Raza et al. [15], depositing materials using 50-μm layer thickness (Fig. 10a), shows that using 75-μm layer thickness seems to give significantly lower amounts of lack of fusion, especially for shorter point distances. It can also be noted that for both 50 and 75-μm bead thickness, there was an increase in the amount of the lack of fusion around 60 μm point distance, indicating that this may be an upper limit of that parameter.

However, most likely, it is not the layer thickness in itself which causes this difference in propensity to form lack of fusion, but rather the deposition characteristics in general. For the 50-μm layer thickness, they were deposited using 115 W laser power and a laser energy varying from 87 to 153 J/mm^3. For the 75-μm layer thickness, the used power was 200 W, but, since the hatch distance was 0.1 mm in this case, the corresponding volumetric energy was 74 to 147 J/mm^3, i.e., somewhat lower than for the 50-μm layer thickness. So even if it is easy to assume that the lack of fusion is due to lack of energy to melt the powder grains, there seems to be at least one further parameter influencing the melting of the powder grains.

Also, the amount of gas porosity varied quite extensively between the two bead thicknesses (Fig. 10b). For the 75 μm, about half of the amount of gas porosity was found. It is not clear, though, whether this is due to less amount of large pores or if it is the general porosity connected to the virgin powder that is less.

The results of micro-indentation for all 25 samples were shown in Fig. 5. As mentioned earlier, for each sample, ten tests were performed to obtain an accurate value of the material hardness. There is a slight increase in hardness with increasing laser energy input. This is fairly difficult to understand, looking only from the metallurgical side. What might happen with increased laser energy input is possibly formation of γ' and γ", which could increase the hardness. Also, less formation of Laves phase could lead to higher contents of solid solution Nb, which could increase hardness somewhat [6, 22]. It is not likely that lack of fusion should give any significant effect on

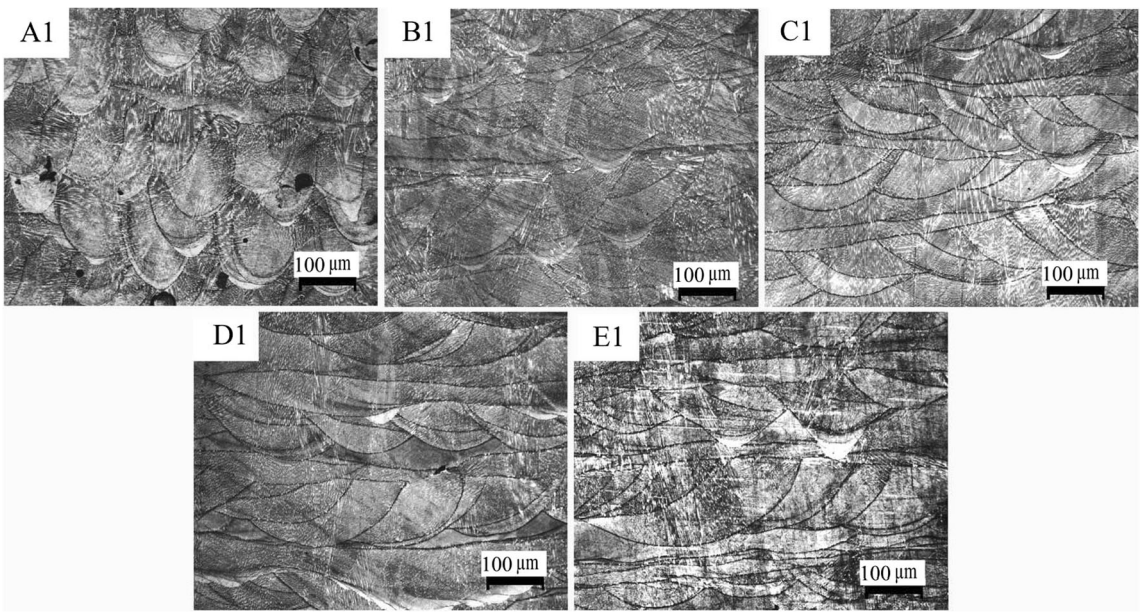

Fig. 7 Optical micrograph of the beads in SLM sample for five different process condition, using the same point distance (40 μm) and different exposure times

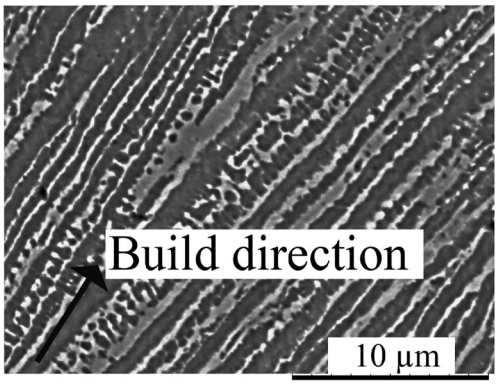

Fig. 8 Representative microstructure of an as-fabricated sample (C1) with laser energy input around 133 J/mm^3

hardness, since the operator normally chooses an area without porosity for doing the hardness indent.

For the 50-µm layer thickness, the hardness varied from just below 310 $HV_{0.5}$ to around 330 $HV_{0.5}$ [15]. In the present study, the hardness varied from around 290 to 320 $HV_{0.5}$, so just below the hardness of the 50-µm layer thickness. But for the 40 µm point distance, of the 50-µm layer thickness, hardness suddenly increased for some combinations of point distance and laser exposure time to relatively high values. Thus, in general, the hardness values for 50- and 75-µm layer thicknesses are quite close, but some odd points are quite far away from the general trend.

The changes in hardness could not be associated with any differences in microstructure. On a coarser level, there was a variation in how the beads appeared, especially between specimen A1 (with the smallest point distance and shortest exposure time) and the other specimens. However, there were otherwise no particular deviations for specimen A1.

The beads varied in width and depth for all specimens, but just the specimens in the four corners were more closely investigated. However, it was not possible to directly couple the width of individual beads to either the point distance or the exposure time of the laser beam. It should of course also be recognized that there was a certain degree of scatter in the size of the beads. The numbers given in Fig. 6 are more an indication of bead sizes found. It is rather difficult to measure a large number of bead sizes in one sample, to get a statistical account of the bead size. Anyhow, it seems as the beads became wider

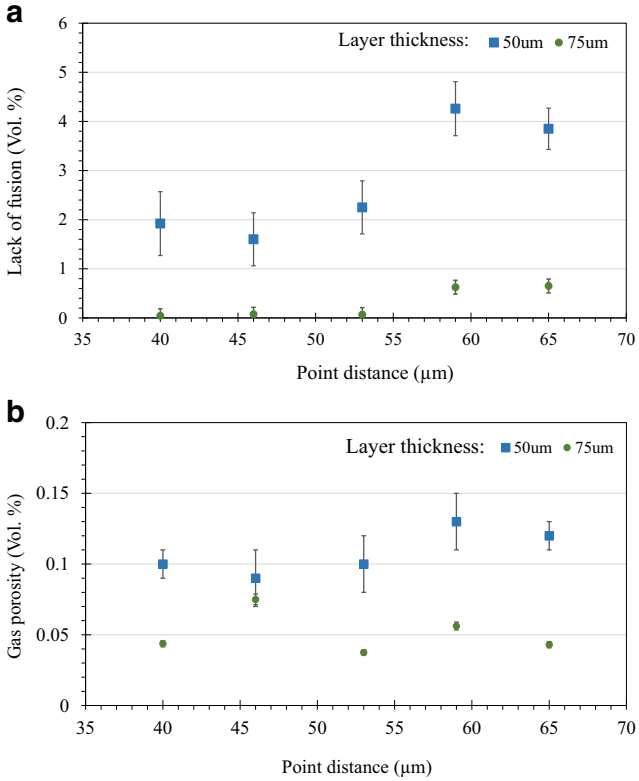

Fig. 10 Effect of point distance on **a** lack of fusion and **b** gas porosity at the exposure time 200 µs in 50 and 75-µm layer thicknesses

and less deep when the point distance was increased, for the same exposure time (cf specimens A1 and A5). When the laser exposure time was increased, for a constant point distance, a significant increase in bead width was seen for a short point distance, while a much smaller increase in bead width was noted for a larger point distance [23]. At present, no explanation for this behavior has been reached.

There was a slight change in coarseness of the microstructure between top and bottom. This trend was noted for all specimens. This is assumed to be related to that the temperature of the deposit is increasing as deposition goes on. For the initial layers, the temperature was pre-set to be 150 °C, but is likely to increase as deposition goes on. However, the final temperature of the deposit is not known, but obviously, the microstructure was somewhat coarser, as shown in Fig. 9. It is consequently also possible that the cooling rate may be slower

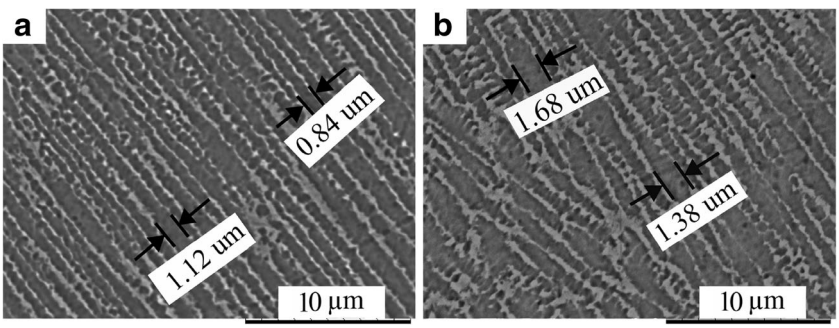

Fig. 9 Microstructure of normal plane from the SLM Alloy 718 sample: **a** bottom layer and **b** top layer (sample A1, laser energy input 120 J/mm^3)

for the later beads in the deposition, compared to the initial beads [24, 25]. This may also lead to a coarser microstructure in the beads higher up in the deposits [26].

It is concluded that more work is needed to understand the variation in microstructure from variations in point distance and laser exposure time. Obviously, there are several factors during deposition that need to be controlled, to achieve a more or less fully dense microstructure. Indeed, the material will be subjected to a HIP process after deposition, but still not too large defects can be present if a suitable material shall emerge after HIP.

5 Conclusions

Selective laser melting process was done for the cubes manufactured specimens from Alloy 718 powder with a layer thickness of 75 μm, using a variety of point distances and laser exposure times. A systematic characterization of microstructural features shows a number of findings which are summarized as follows:

- Total porosity is found to be a function of laser energy input. By increasing laser energy input, it was decreasing. The minimum amount of porosity was observed at 122 J/mm^3.
- Large lack of fusion was found in most of the specimen, but most commonly in those with large point distances (65 μm) and short exposure time (180 μs).
- Lower amount of lack of fusion was found in 75-μm-thick layers than in 50-μm-thick layers with the same laser energy input, particularly for small point distances.
- Porosity was also found, but on a lower level than lack of fusion and mostly without any coupling to process data.
- Hardness increased slightly with increased laser energy input.
- The width of the deposited beads increased with increased laser energy.
- In the light of the present study, by using low point distance (40–53 μm) and high exposure time (200–220 μs), a denser material can be obtained.

Acknowledgements The authors gratefully acknowledge the financial support from The Swedish National Space Board and VINNOVA (National Space Research Program and National Aviation Engineering Research Program). The authors also would like to thank Mr. Esmaeil Sadeghimeresht and Mr. Kenneth Andersson for sharing their knowledge in material preparation and microstructural analysis. Mr. Staffan Brodin and Mr. Magnus Holmquist from GKN Aerospace Sweden AB are acknowledged for their scientific support.

References

1. Zhao X, Chen J, Lin X, Huang W (2008) Study on microstructure and mechanical properties of laser rapid forming Inconel 718. Mater Sci Eng A 478(1–2):119–124
2. Fu SH, Dong JX, Zhang MC, Xie XS (2009) Alloy design and development of INCONEL718 type alloy. Mater Sci Eng A 499(1–2):215–220
3. Blackwell PL (2005) The mechanical and microstructural characteristics of laser-deposited IN718. J Mater Process Technol 170(1–2):240–246
4. Wang Z, Guan K, Gao M, Li X, Chen X, Zeng X (2012) The microstructure and mechanical properties of deposited-IN718 by selective laser melting. J Alloys Compd 513:518–523
5. Jia Q, Gu D (2014) Selective laser melting additive manufactured Inconel 718 superalloy parts: high-temperature oxidation property and its mechanisms. Opt Laser Technol 62:161–171
6. Jia Q, Gu D (2014) Selective laser melting additive manufacturing of Inconel 718 superalloy parts: densification, microstructure and properties. J Alloys Compd 585:713–721
7. Lu Y et al (2015) Study on the microstructure, mechanical property and residual stress of SLM Inconel-718 alloy manufactured by differing island scanning strategy. Opt Laser Technol 75:197–206
8. Song B et al (2015) Differences in microstructure and properties between selective laser melting and traditional manufacturing for fabrication of metal parts: a review. Front Mech Eng 10(2):111–125
9. Li R, Liu J, Shi Y, Wang L, Jiang W (2012) Balling behavior of stainless steel and nickel powder during selective laser melting process. Int J Adv Manuf Technol 59(9–12):1025–1035
10. Xia M, Gu D, Yu G, Dai D, Chen H, Shi Q (2017) Porosity evolution and its thermodynamic mechanism of randomly packed powder-bed during selective laser melting of Inconel 718 alloy. Int J Mach Tools Manuf 116:96–106
11. Choi J-P et al (2017) Densification and microstructural investigation of Inconel 718 parts fabricated by selective laser melting. Powder Technol 310:60–66
12. Yadroitsev I, Smurov I (2010) Selective laser melting technology: from the single laser melted track stability to 3D parts of complex shape. Phys Procedia 5:551–560
13. Ma M, Wang Z, Gao M, Zeng X (2015) Layer thickness dependence of performance in high-power selective laser melting of 1Cr18Ni9Ti stainless steel. J Mater Process Technol 215:142–150
14. Sufiiarov VS, Popovich AA, Borisov EV, Polozov IA, Masaylo DV, Orlov AV (2017) The effect of layer thickness at selective laser melting. Procedia Eng 174:126–134
15. Raza T, Andersson J, Svensson L-E (2017) Influence of laser 448 exposure time and point distance on microstructure, porosity and hardness of selective laser melted Alloy 718. Addit Manuf. Under review
16. ASTM Standard E562-08 (2008) Test method for determining volume fraction by systematic manual point count. ASTM International, West Conshohocken, PA. https://doi.org/10.1520/E0562-11. www.astm.org
17. Wang X, Gong X, Chou K (2016) Review on powder-bed laser additive manufacturing of Inconel 718 parts. Proc Inst Mech Eng, Part B: J Eng Manuf 231(11):1890-1903
18. Thijs L, Verhaeghe F, Craeghs T, Humbeeck JV, Kruth J-P (2010) A study of the microstructural evolution during selective laser melting of Ti–6Al–4V. Acta Mater 58(9):3303–3312

19. Kasperovich G, Haubrich J, Gussone J, Requena G (2016) Correlation between porosity and processing parameters in TiAl6V4 produced by selective laser melting. Mater Des 105:160–170
20. Amato KN et al (2012) Microstructures and mechanical behavior of Inconel 718 fabricated by selective laser melting. Acta Mater 60(5): 2229–2239
21. Helmer HE, Körner C, Singer RF (2014) Additive manufacturing of nickel-based superalloy Inconel 718 by selective electron beam melting: processing window and microstructure. J Mater Res 29(17):1987–1996
22. PAN X, YU H, TU G, SUN W, HU Z (2011) Segregation and diffusion behavior of niobium in a highly alloyed nickel-base superalloy. Trans Nonferrous Met Soc China 21(11):2402–2407
23. Cherry JA, Davies HM, Mehmood S, Lavery NP, Brown SGR, Sienz J (2015) Investigation into the effect of process parameters on microstructural and physical properties of 316L stainless steel parts by selective laser melting. Int J Adv Manuf Technol 76(5–8): 869–879
24. Gong X, Wang X, Cole V, Jones Z, Cooper K, Chou K (2015) Characterization of microstructure and mechanical property of Inconel 718 from selective laser melting. Proceedings of the ASME 2015 International Manufacturing Science and Engineering Conference MSEC2015, Charlotte, North Carolina, USA
25. Wu X, Liang J, Mei J, Mitchell C, Goodwin PS, Voice W (2004) Microstructures of laser-deposited Ti–6Al–4V. Mater Des 25(2): 137–144
26. Bontha S, Klingbeil NW, Kobryn PA, Fraser HL (2009) Effects of process variables and size-scale on solidification microstructure in beam-based fabrication of bulky 3D structures. Mater Sci Eng A 513–514:311–318